

## Characterization of Arcjet Type Arc-Heater Plumes

33rd Plasmadynamics and Lasers Conference  
20-23 May 2002, Maui, Hawaii

AIAA 2002-2242

Makoto MATSUI,\* Kimiya KOMURASAKI,† and Yoshihiro ARAKAWA‡

The university of Tokyo, Hongo 7-3-1, Bunkyo, Tokyo 113-0033, Japan

### Abstract

Laser absorption spectroscopy has been applied to the measurement of arc-heater plumes. Number density distribution of metastable atomic oxygen was obtained from the measured absorption line profile at 777.19 nm in argon-oxygen plumes generated by arcjet type arc-heaters. As a result, oxygen is found localized off axis at the nozzle exit, and diffusing from outside to the axis in the plume. Moreover, CFD simulation was conducted to investigate the mixing process of oxygen in the arc-heater. The result indicates that the degree of oxygen dissociation in the plume would be at the level of 0.01%.

### INTRODUCTION

In developing Thermal Protection Systems for reentry vehicles, arc-heaters are often used to simulate reentry conditions. Arcjet type arc-heaters<sup>1-3)</sup> and segmented cathode type arc-heaters<sup>4,5)</sup> are widely used. The segmented cathode type has an advantage of high input power as shown in Table 1 because it can sustain long arc discharge. However, it takes several hours for maintenance after a few minutes operation. On the other hand, the arcjet type requires almost no maintenance after several-hour operation. Therefore, arcjet type arc-heaters are convenient for basic TPS studies.

However, their exact plume conditions are mostly unknown because they are usually in strong thermo-chemical nonequilibrium. Although non-intrusive spectroscopic methods such as emission spectroscopy and Laser Induced Fluorescence have been actively applied to the characterization of such high enthalpy plumes, and the excitation, vibration, and rotational temperatures of atoms and molecules in the plumes are gradually clarified,<sup>6-9)</sup> it is still difficult to measure the chemical compositions by these spectroscopic methods.

Recently, atomic oxygen in the flow is recently found to play important roles in TPS tests through the heat-flux enhancement by recombination reactions and the active-passive oxidation.<sup>10)</sup>

Therefore, in this research, laser absorption spectroscopy method<sup>11-12)</sup> is applied to examine the number density distribution of atomic oxygen in the arcjet type arc-heater plumes along with CFD analysis.

\* Graduate Student, Department of Advanced Energy

† Associate Professor, Department of Advanced Energy, Member AIAA, kimiya@k.u-tokyo.ac.jp

‡ Professor, Department of Aeronautics and Astronautics, Member AIAA

Copyright © 2001 The American Institute of Aeronautics and Astronautics Inc. All right reserved.

**Table 1 Arc-heater.**

| Institute           | Type      | Power [MW] |
|---------------------|-----------|------------|
| JUTEM <sup>2)</sup> | Arcjet    | 0.02       |
| IRS <sup>3)</sup>   | Arcjet    | 1.0        |
| ISAS <sup>4)</sup>  | Segmented | 1.0        |
| NASA <sup>5)</sup>  | Segmented | 20         |

### EXPERIMENTAL METHOD

#### Arc-heaters

The schematics of arcjet type arc-heaters developed at the Japan Ultra-high Temperature Materials research center (JUTEM) and at the university of Tokyo are shown in Figs. 1 and 2, respectively. In both of the arc-heaters, inert gas such as argon or nitrogen is supplied from the base of cathode rod. Oxygen is added at the constrictor part to prevent the cathode from oxidation.

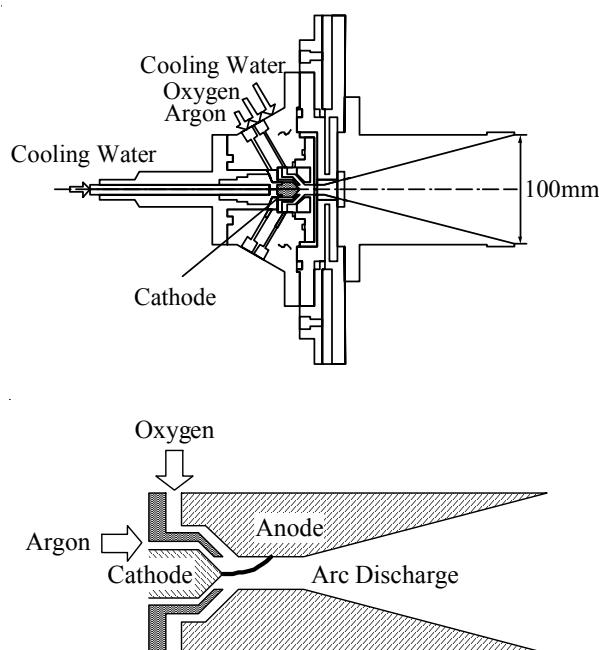


**Fig. 1 JUTEM arc-heater (upper) and the zoom up of constrictor part (below.)**

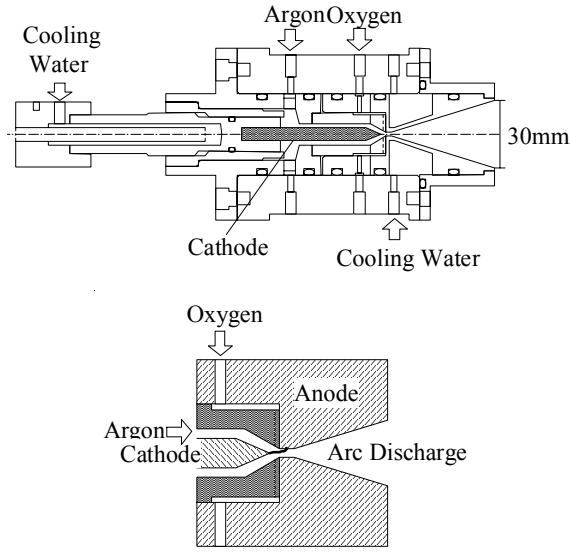


**Fig. 2 The university of Tokyo arc-heater (upper) and the zoom up of constrictor part (below.)**

### Laser absorption spectroscopy

Laser absorption spectroscopy has some superiority to the emission and LIF spectroscopy: 1) it is applicable to optically thick plasma, and 2) absolute calibration using a standard light source or a density reference cell is not necessary. Moreover, 3) the measurement system is portable when a diode laser is used.

In this research, the number density of atomic oxygen is measured using the absorption profile of the OI transition from  $3s^5S_2$  to  $3p^5P_3$  at the wavelength of 777.19nm. Its lower state is a metastable state as shown in Fig. 3.

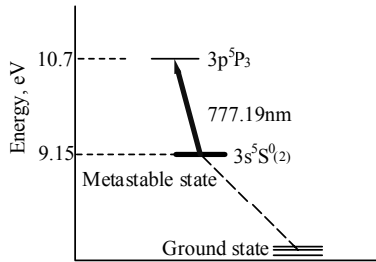


**Fig. 3 Energy level diagram of atomic oxygen.**

The relationship between laser intensity  $I_\nu$  and absorption coefficient  $k_\nu$  is expressed by the Beer-Lambert law as,

$$\frac{dI_\nu}{dx} = -k_\nu I_\nu \quad (1)$$

Here,  $\nu$  is frequency of the laser light. Assuming axisymmetric distribution of absorption properties in plumes, local absorption coefficient is obtained by the Abel inversion as

$$k_\nu(r) = \frac{1}{\pi} \int_{-r}^r \frac{d \left( \ln \frac{I_\nu(y)}{I_{\nu 0}} \right)}{dy} \frac{dy}{\sqrt{y^2 - r^2}} \quad (2)$$

Here,  $y$  is a coordinate in the scan direction of the probe laser (perpendicular to the laser path and the flow), and  $r$  is the radial coordinate in the cylindrical coordinate system applied to the axisymmetric plume. Since the local absorption is a sum of an absorption coefficient and a stimulated emission coefficient, the relationship between integrated absorption coefficient  $K(r)$  and population density at the absorbing state  $n_1$  is given as

$$K = \int_{-\infty}^{\infty} k_\nu d\nu = \frac{\lambda^2}{8\pi} \frac{g_2}{g_1} A_{21} n_1 \left[ 1 - \exp\left(-\frac{\Delta E_{12}}{kT_{ex}}\right) \right] \quad (3)$$

Here, 1 denotes the absorbing level and 2 does the excited level.  $\Delta E_{12}$  is the energy gap between levels 1 and 2, and  $T_{ex}$  is the electronic excitation temperature. At 777.19 nm,  $\Delta E_{12}/k$  is 18,500 K. If  $T_{ex} < \Delta E_{12}/k$ , stimulated emission can be neglected and Eq. (3) is simplified as

$$K = \frac{\lambda^2}{8\pi} \frac{g_2}{g_1} A_{21} n_1 \quad (4)$$

Here,  $\lambda$  is an absorption wavelength,  $g$  is a statistical weight and  $A$  is an Einstein coefficient. At 777.19nm,  $g_1=5$ ,  $g_2=7$  and  $A_{21}=3.69 \times 10^7 s^{-1}$ .

### Experimental apparatus and conditions

The schematic of measurement system is shown in Fig. 4. A tunable diode-laser with an external cavity was used as a laser oscillator. The laser beam is divided into three beams by beam splitters. The first beam is directly detected by a photo-detector as a reference signal. The second is detected through an etalon whose free spectral range is 1 GHz. The third is lead to a window of vacuum chamber through a multimode optical fiber. The fiber output is mounted on a one-dimensional traverse stage to scan the plume in the radial direction of the plume. At the other side of the chamber, the laser beam is focused on a detector using a parabola mirror. This makes it possible to detect the probe laser without synchronizing the detector position with the laser scanning.

The test conditions are listed in Table 2. Argon and oxygen are used as a working gas. In this gas mixture, high degree of oxygen dissociation is expected due to the dissociation collision with excited argon atoms. The photograph of the plumes is shown in Figs. 5 and 6.

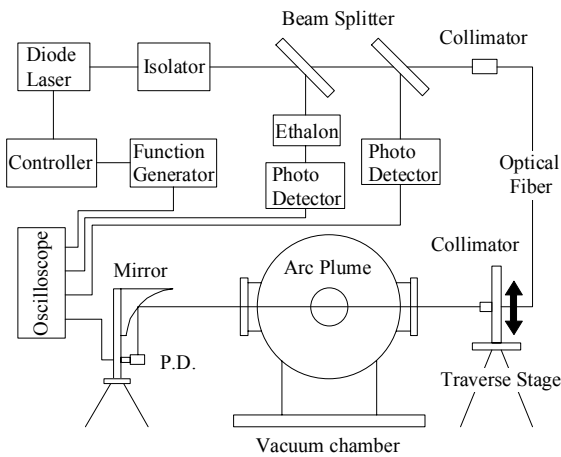


Fig. 4 Schematic of measurement system.

Table 2 Test conditions.

| Institute           | Gas flow                                | Specific enthalpy | Back pressure |
|---------------------|---|-------------------|---------------|
| JUTEM               | Ar: 20[slm]<br>O <sub>2</sub> : 5[slm]  | 6.1 [MJ/kg]       | 38 [Pa]       |
| University of Tokyo | Ar: 6[slm]<br>O <sub>2</sub> : 1.5[slm] | 3.3 [MJ/kg]       | 26 [Pa]       |

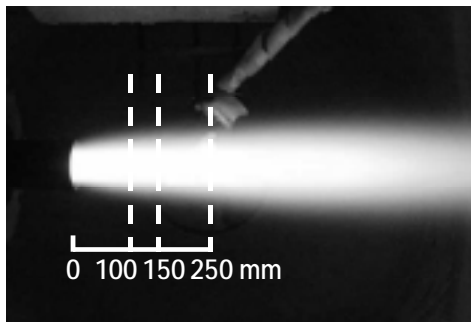


Fig. 5 JUTEM arc-heater plume.

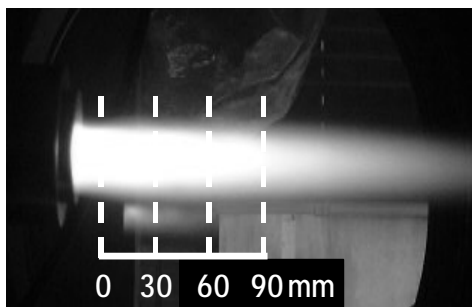


Fig. 6 The university of Tokyo arc-heater plume.

### EXPERIMENTAL RESULTS

The number density distribution of metastable atomic oxygen in the JUTEM arc-heater plume is

shown in Fig. 7. Here,  $z$  and  $r$  are defined by the cylindrical coordinate and origin is taken at the center of nozzle exit.

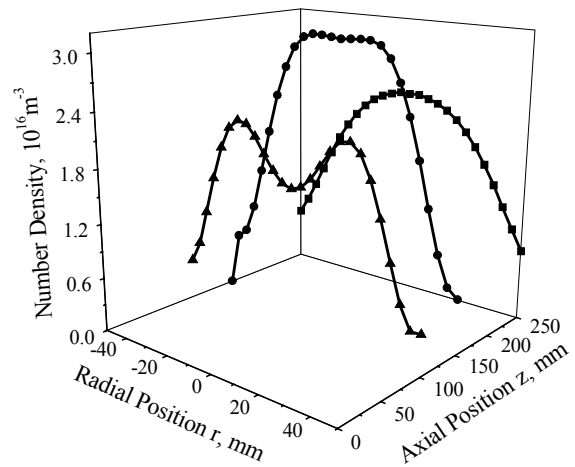


Fig. 7 Number density distribution of metastable atomic oxygen in the JUTEM arc-heater plume.

At  $z=100$ mm, the peak of number density is located off axis at  $r=24$ mm. Then, the peak approaches to the axis in the downstream of the plume and finally the peak is located on the axis at  $z=250$ mm. The maximum number density in each plane increases up to  $3 \times 10^{16} \text{m}^{-3}$  at  $z=150$ mm and then decreases.

The number density distribution of metastable atomic oxygen in the university of Tokyo arc-heater plume is shown in Fig. 8. Similarly to the JUTEM arc-heater plume, the peak is also located off axis at the exit of the nozzle, and then the peak approaches to the axis in the downstream of the plume with the increase in number density.

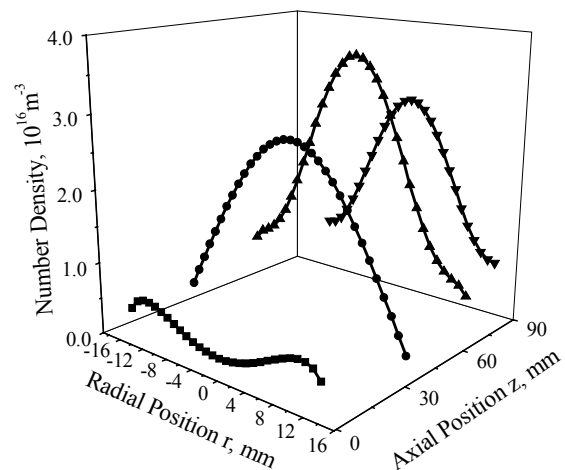
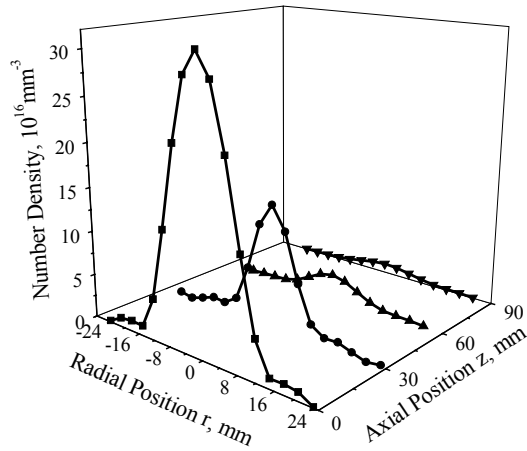


Fig. 8 Number density distribution of metastable atomic oxygen in the university of Tokyo arc-heater plume.

Figure 9 shows the number density distribution of metastable argon. (It was measured using an ArI

absorption line at 842.82nm.) It has a peak on the axis at the nozzle exit and then the number density decreases rapidly in the downstream of the plume.



**Fig. 9** Number density distribution of the metastable argon in the university of Tokyo arc-heater plume.

Consequently, oxygen is localized off axis near the nozzle exit and diffuses to the axis in the downstream region while it is dissociating. On the other hand, the metastable argon number density has a peak on the axis at the nozzle exit and decreases rapidly due to quenching in the downstream region. Therefore, it is thought that oxygen is not enough mixed with argon and not dissociated in the constrictor region. The hypothetical oxygen-argon mixing process in the plume is schematically shown in Fig. 10.

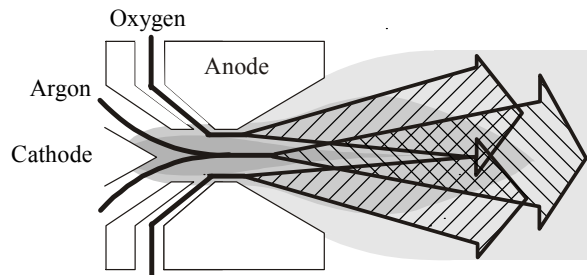


**Fig. 10** Hypothetical oxygen-argon mixing process.

### CFD ANALYSIS

The number density of ground state atomic oxygen is difficult to be deduced from that of metastable state one because its electronic excitation would not be in equilibrium. Therefore, it was estimated by CFD simulations. In the conventional CFD analyses on an arcjet type arc-heater,<sup>13,14)</sup>

oxygen mixing process has not been taken into account.

### Numerical models

Since the simulation focuses on the diffusion and mixing processes of the oxygen injected at the constrictor part, arc discharge process has not been solved for simplicity. The temperature distribution of the inlet argon flow was given as a boundary condition assuming thermo-chemical equilibrium. This assumption would be valid because the flow speed is subsonic and pressure is high in the region around the cathode tip. The temperature profile has a sharp peak on the axis to simulate the cathode jet phenomena.

Seven species and seven chemical reactions model is used in this calculation as listed in Table 3. Arrhenius type forward reaction rates were used and the principle of the detailed balance was used to have backward reaction rates. One temperature model is employed.

**Table 3** Chemical reaction models.

| Reaction process  | Reference |
|---|-----------|
| Ar + e → Ar <sup>+</sup> + e + e                                  | (15)      |
| O <sub>2</sub> + Ar → O + O + Ar                                  | (15)      |
| O <sub>2</sub> + O → O + O + O                                    | (16)      |
| O <sub>2</sub> + O <sub>2</sub> → O + O + O <sub>2</sub>          | (16)      |
| O + e → O <sup>+</sup> + e + e                                    | (16)      |
| O + O → O <sub>2</sub> <sup>+</sup> + e                           | (16)      |
| O + O <sub>2</sub> <sup>+</sup> → O <sub>2</sub> + O <sup>+</sup> | (16)      |

Viscosity  $\mu$ , thermal conductivity  $\kappa$  and diffusion coefficient  $D$  were calculated by the formulas in reference 16. In the free jet region, the algebraic turbulence model by the Plandtl's mixing length theory was used. The Reynolds number at the nozzle exit was 1800.

### Governing Equations

The fundamental equations are two-dimensional axisymmetric Navier-Stokes equations extended to chemical nonequilibrium gases shown as,

$$\frac{\partial \mathbf{Q}}{\partial t} + \frac{\partial \mathbf{F}}{\partial z} + \frac{\partial \mathbf{G}}{\partial r} + \mathbf{H} = \frac{\partial \mathbf{F}_v}{\partial z} + \frac{\partial \mathbf{G}_v}{\partial r} + \mathbf{S} \quad (5)$$

Here,  $\mathbf{Q}$  is conservative term,  $\mathbf{F}$ ,  $\mathbf{G}$  are convection flux terms,  $\mathbf{F}_v$ ,  $\mathbf{G}_v$  are viscous terms,  $\mathbf{H}$  is term related to three dimensional convergent effect in Eq. (5) and  $\mathbf{S}$  is chemical source term shown as,

$$\mathbf{Q} = \begin{bmatrix} \rho \\ \rho u \\ \rho v \\ e \\ \rho_1 \\ \vdots \\ \rho_7 \end{bmatrix}, \quad \mathbf{F} = \begin{bmatrix} \rho u \\ \rho u^2 + p \\ \rho uv \\ (e+p)u \\ \rho_1 u \\ \vdots \\ \rho_7 u \end{bmatrix}, \quad \mathbf{F}_v = \begin{bmatrix} 0 \\ \tau_{zz} \\ \tau_{zr} \\ \tau_{zz}u + \tau_{zr}v + \kappa T_z \\ -D_1 X_{1,z} \\ \vdots \\ -D_7 X_{7,z} \end{bmatrix}$$

$$\mathbf{H} = \frac{1}{r} \begin{bmatrix} \rho v \\ \rho uv + \tau_{zr} \\ \rho v^2 + \tau_{rr} - \tau_{\theta\theta} \\ (e+p)v - \kappa T_r - u\tau_{zr} - u\tau_{rr} \\ \rho_1 v + D_1 X_{1,r} \\ \vdots \\ \rho_7 v + D_7 X_{7,r} \end{bmatrix}, \quad \mathbf{S} = \begin{bmatrix} 0 \\ 0 \\ 0 \\ 0 \\ \dot{\rho}_1 \\ \vdots \\ \dot{\rho}_7 \end{bmatrix}$$

Here,  $\rho$  is density,  $u$ ,  $v$  are axial and radial components of velocity,  $e$  is specific energy,  $p$  is pressure,  $\tau$  is viscous stress,  $T$  is temperature and  $X$  is mole fraction.

The convection terms were calculated using the SHUS (Simple High-resolution Upwind Scheme,) in which the spatial accuracy is extended to third order using the MUSCL approach. Implicit time integration has been done using the LU-SGS (Lower-Upper Symmetric Gauss Seidel Scheme.)

### Computation conditions

The schematic of computational grid for the university of Tokyo arc-heater plume analysis is shown in Fig. 11. A similar grid was used for the JUTEM arc-heater plume analysis. The calculation region is composed of two sections; the constrictor-nozzle section and the free jet section. At the interface of these sections, several computational grids were superposed to preserve the spatial accuracy. Since entire region in the constrictor and nozzle is covered by boundary layers, it is not necessary to concentrate the grid points near the wall surface.

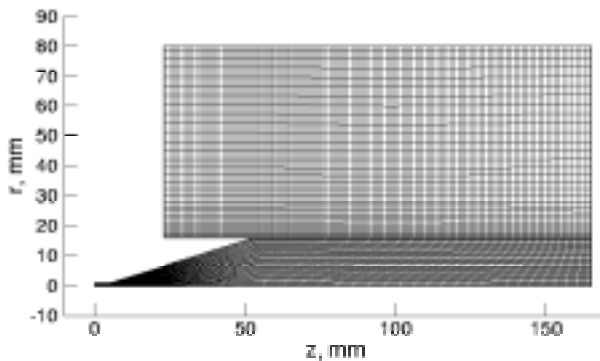


Fig. 11 A computational grid.

The grid spacing in the radial direction should be so small that the numerical dissipation effect becomes smaller than actual diffusion. The grid dependence is shown in Fig. 12. The full width at half maximum of argon number density profile at  $z=10\text{mm}$  is plotted. At this position, the grid spacing should be less than 1.3mm. In this case, total number of the grid points is about 10,000.

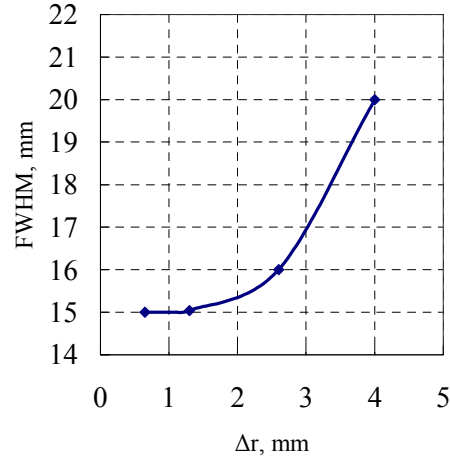


Fig. 12 Grid dependence.

The operational conditions listed in Table 2 are used for the computations. The inlet velocity of argon flow is subsonic so that the inlet pressure is extrapolated from the inside of constrictor. The pressure extrapolation is also done at the oxygen injection slit. To simulate the high temperature cathode jet, the Gaussian temperature distribution is assumed at the inlet as shown in Fig.13. The degree of ionization of argon at the inlet was computed assuming the Saha equilibrium. As for the wall of the constrictor, nozzle and chamber, adiabatic non-slip wall conditions were used.

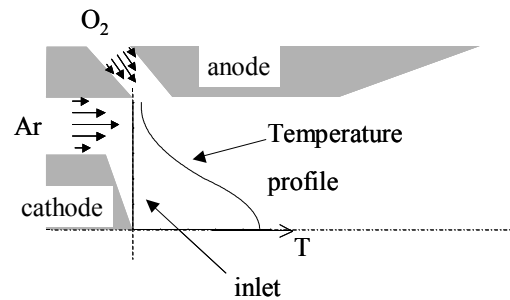
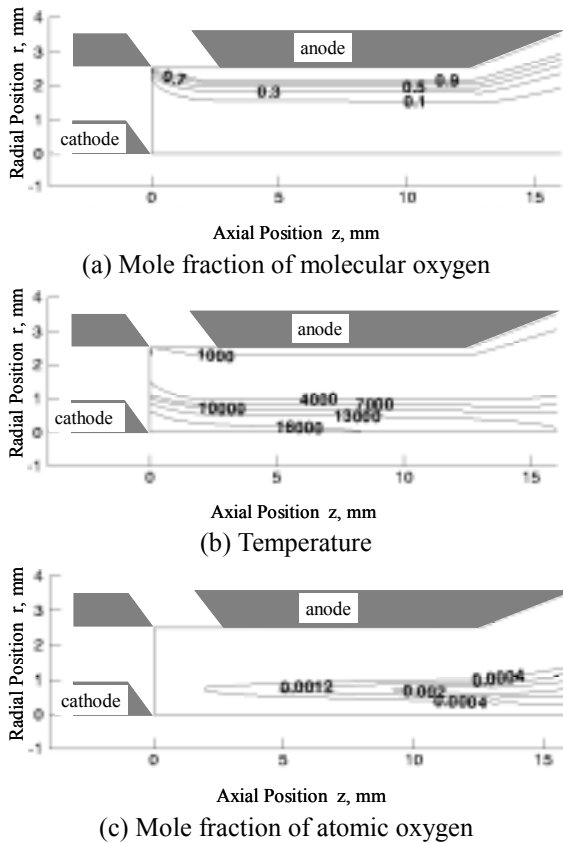


Fig. 13 Gas inlet conditions.

### ANALYTICAL RESULTS AND DISCUSSION

The contours of  $\text{O}_2$  mole fraction, temperature and  $\text{O}$  mole fraction in the constrictor part of the JUTEM arc-heater are shown in Fig. 14 and the radial distributions of these properties at 10 mm downstream from the cathode tip are plotted in Fig.

15.



**Fig. 14** Contours of the computed gas properties in the constrictor.

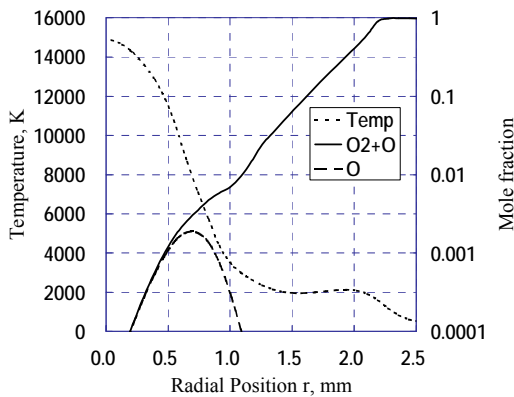


**Fig. 15** Radial distributions of temperature and oxygen mole fractions in the constrictor.

Since oxygen mixing is very slow, oxygen concentration is localized outside part of the plume in the constrictor. On the other hand, the temperature distribution still has a peak on the axis. Although the degree of dissociation is high in the region of  $r < 0.7$  mm, number density of atomic oxygen is very small. The average degree of dissociation at this cross section is as small as 0.01%.

The computed number density distribution of atomic oxygen in the JUTEM arc-heater plume is

shown in Fig. 16. It corresponds to the case as previously shown in Fig. 7. The distribution has a peak at  $r=20$  mm and the peak approaches to the axis in the downstream of the plume. The maximum number density in each plane increases from  $z=100$  mm to 150 mm. Consequently, localized oxygen distribution was also obtained in the simulation. This would be the reason why the measured metastable oxygen distribution has a peak off axis.

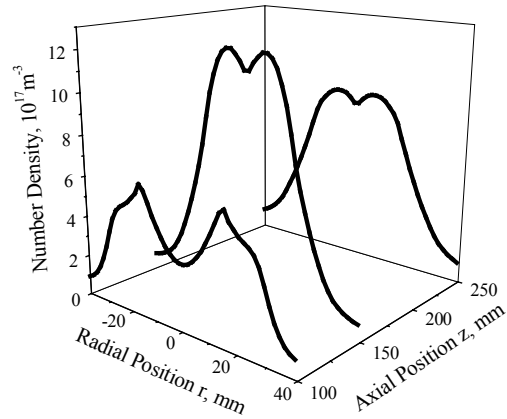


**Fig. 16** Computed number density distribution of atomic oxygen in the JUTEM arc-heater plume.

The similar results were obtained for the university of Tokyo arc-heater plume. Figure 17 shows the computed contours of number density of atomic oxygen in the university of Tokyo arc-heater plume. Although the oxygen is mixing in the plume, the reaction rate is quite small because of the decrease in temperature. In the plume, computed temperature is the level of 2,000 K on the axis. Therefore, the atomic oxygen number density did not increase very much. The average dissociation degree of the oxygen in the plume was estimated at 0.01%.

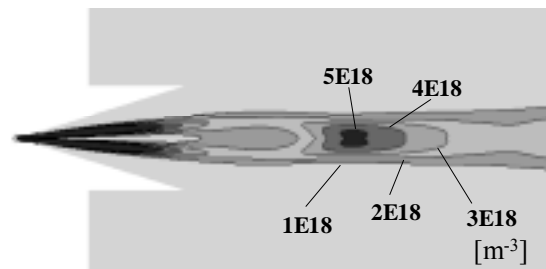


**Fig. 17** Computed contours of number density of atomic oxygen in the university of Tokyo arc-heater plume.

As mentioned above, the dissociation of oxygen is hardly expected in the plume. Therefore, it is necessary to promote the mixing in the constrictor region to obtain the high degree of oxygen

dissociation.

### CONCLUSION

- The distributions of metastable and total atomic oxygen number density were obtained by the laser absorption spectroscopy and the CFD simulation, respectively.
- Oxygen injected at the constrictor is found not enough mixed with argon in the constrictor, resulting in the quite small degree of dissociation of oxygen in the plume.

### REFERENCE

- 1) Nishida, M. and Watanabe, Y.: Preliminary Experiments of Atomic Oxygen Generation for Space Environmental Testing, *Trans. Japan Soc. Aero. and Space Sci.*, Vol.31, No.93 (1998), p123-133.
- 2) Ishii, M., Ito, M., Toki, K. and Kuriki, K.: Atomic Oxygen Flow Facility Using Arcjet, Proceedings of 16 th Int'l Symp. on Space Tech. and Sic., Vol.1 (1988), p363-368.
- 3) Auweter-Kurtz, M., Kurtz, H. and Laure, S.: Plasma Generators for Re-Entry Simulation, *Journal of Propulsion and Power*, Vol. 12, No. 6 (1996), pp.1053-1061.
- 4) Salinas, I. T., Park, C., Strawa, A. W., Gopaul, N. and Taunk, J. S.: Spectral Measurements in the Arc Column of an Arc-Jet Wind Tunnel, AIAA Paper 94-2595, 1994.
- 5) Hinada, M., Inatani, Y., Yamada, T. and Hiraki, K.: An Arc-Heated High Enthalpy Test Facility for Thermal Protection Studies, ISAS-RN-664.
- 6) Hirakawa, M., Abe, K., Nishida, M., Takeishi, K. and Itoh, K.: Measurement of emission spectra from a shock layer of a blunt body in arc-heated gas, AIAA Paper 2001-1760, 2001.
- 7) Lago, V., Lebehot, A., Dudeck, M., Pellerin, S., Renault, T., and Echegut, P.: Entry Conditions in Planetary Atmospheres: Emission Spectroscopy of Molecular Plasma Arcjets, *Journal of Thermophysics and Heat Transfer*, Vol. 15, No. 2 (2001), pp.168-175.
- 8) Winter, M. W. and Auweter-Kurtz, M.: Boundary Layer Investigation in front of a Blunt Body in a Subsonic Air Plasma Flow by Emission Spectroscopic Means, AIAA paper 98-2460, 1998.
- 9) Storm, P. V. and Cappelli, M. A.: Laser-induced fluorescence measurements within an arcjet thruster nozzle, AIAA Paper 95-2381, 1995.
- 10) Kurotaki, T.: Construction of Catalytic Model on SiO<sub>2</sub> Based Surface and Application to Real Trajectory, AIAA Paper 2000-2366, 2000.
- 11) Arroyo, M. P., Langlogis, S. and Hanson, R. K.: Diode-laser absorption technique for simultaneous measurement of multiple gasdynamic parameters in high-speed flows containing water vapor, *Applied Optics*, Vol. 33 (1994), pp.3296-3370.
- 12) Zhang, F. Y., Komurasaki, K., Iida, T., and Fujiwara, T.: Diagnostics of an argon arcjet plume with a diode laser, *Applied Optics*, Vol. 38 (1999), pp1814-1822
- 13) Auweter-Kurtz, M., Goltz, T., Habiger, H., Hammer, F., Kurtz, H., Riehle, M. and Sleziona, C.: High-Power Hydrogen Arcjet Thrusters, *Journal of Propulsion and Power*, Sep., Vol.14, No.5 (1988) , pp. 764-773.
- 14) Matsuzaki, R. and Hirabayashi, N.: Some Characteristics of the Arc-Heater, Nozzle Flow, and the Underexpansion Jet in the NAL 60kW Plasma Wind Tunnel, NAL TR-307.
- 15) Matsuzaki, R.: Quasi- One-Dimensional Aerodynamics with Chemical, Vibrational and Thermal Nonequilibrium, *Transactions of Japan Society of Aeronautics and Space Science*, Vol.30, No.90 (1988), pp243-258.
- 16) Guputa, R. N. Yos, J. M. Thompson, R. A., and Lee, K. P.: A Review of Reaction Rates and Thermodynamic and Transport Properties for an 11-Species Air Model for Chemical and Thermal Nonequilibrium Calculations to 30000K, NASA R.P 1232, 1990.